# Compact isolation of a large mirror at low frequency

**A. Sider** [1], **T. Dehaeze** [1,3], **J. Watchi** [2], **M. H. Lakkis** [1,2], **R. Jamshidi** [1], **A. Amorosi** [1,2], **L. Amez-Droz** [1,2], **M. Teloi** [2], **C. Collette** [1,2]
[1] Université de Liège, PML - Precision Mechatronics Laboratory,
B-4000 Liège, Belgium

[2] Free University of Brussels, Beams, Precision Mechatronics Laboratory
Avenue F.D. Roosevelt 50, B-1050, Brussels, Belgium

[3] ESRF - European Synchrotron Radiation Facility
Avenue des Martyrs, CS 40220, 38043, Grenoble, France

## Abstract
This study presents a compact isolation system of a large mirror at low frequency. The work is carried out in the framework of the E-TEST project to investigate a new concept of design for the future Einstein Telescope (Europe's next-generation gravitational-wave detector). The isolation system combines an active inertial platform, a passive inverted pendulum platform, and a multi-cascaded pendulum in one system. Given that, the study addresses the isolation system design, its dynamics, and the applied control strategy. For the control strategy, a decoupling method based on a geometric approach is first applied to reduce the magnitude of the off-diagonal elements of the transfer matrix. Then the controller is applied in the Cartesian frame based on the loop shaping method. The simulation results show that the seismic noise could be reduced by about 3 orders of magnitude at 1 Hz in the horizontal and vertical directions when the control is applied. It is also shown that the control is still performing well despite of the residual coupling of the inertial sensor.

## 1 Introduction

With the aim of detecting Gravitational Waves (GWs) to discover hidden things in this universe, the researchers and Scientifics came out with an extraordinary sensitive laser interferometer detector [1]. One of the limitations of this measurement system is the seismic noise which results either from natural phenomena (such as the waves of the ocean) or from human activities (such as the movement of the vehicles) [2, 3]. The seismic noise causes a tiny displacement of the mirror, which is one of the main parts of the measurement system, hence degrading the performance of the measurements. The amount of the resulted displacement depends on the level of the seismic noise which varies around the world and also during the day. The mirror, therefore, has to be isolated from such noise in the frequency bandwidth of interest to be able to detect a tiny displacement for example in the order of $10^{-18}\ m$ [3]. Besides, the isolation system provides an essential mean for the positioning control as well as for the compensation of the swinging angle of the measurement system [4].

There are currently three main ground-based GW detectors being operated with different isolation systems: advanced LIGO in USA [5], advanced Virgo in Italy [6] and KAGRA in Japan [7]. Unlike usual isolation system, the GW isolation system is a set of sub-isolation systems that are combined to improve the overall seismic noise suppression. For example, Advanced LIGO has designed two main isolation systems in its observatory detectors [8]. These isolators are based on a combination of active-passive isolators. The first isolation system (5.5 m height) contains three cascaded systems with an overall of seven stages of seismic isolation: HEPI (pre-active isolator), two stages of BSC-ISI (main active isolators), and four cascaded pendulum-masses (passive isolators) that are mounted on HEPI [9]. The second isolation system (2 m height) consists of three cascaded systems with an overall five stages of seismic isolation: HEPI (pre-active isolator),

HAM-ISI (main active isolator), and three cascaded pendulum-masses (passive isolators) that are mounted on HAM-ISI. In addition to their compactness, the LIGO isolation systems provide an extra seismic noise attenuation below the resonance of the structure due to the inertial active platform [8]. The experimental result shows that the first isolation system of the LIGO could yield isolation in the amplitude of about a factor of 300 at 1 Hz and about 3000 at 10 Hz [8]. The performance of this approach however is limited at low-frequency bandwidth where the seismic noise attenuation is difficult to be obtained. This is due to the sensor noise, sensor coupling and coupling due to the gravity [2, 8, 10]. Beside, this approach needs additional means to position the entire isolation system and compensate for the tidal drift [9]. This adds complexity to the system which is not the case if the Inverted Pendulum Platform (IPP) is used in the isolation system [11, 4].

On the other side, the isolation system of the Advanced Virgo (known as Superattenuator) applies a combination of only passive isolators that contains one IPP [12], five cascaded pendulum mechanical filters and three cascaded pendulum-masses for the payload (steering filter, marionette (for position control at frequencies 10 mHz and larger) and mirror) [13]. The isolation design of the ET is also inspired from the Superattenuator but with an upgraded model to achieve the desired sensitivity requirement of the ET (desired horizontal cross-over frequency around 1.8 Hz) [14, 15]. This results in a 17.5 m height isolation system [14].

Similarly, the KAGRA isolation system relies on a combination of passive isolators for the seismic noise suppression [16]. It has implemented four isolation types (Type-A, Type-B, Type-Bp, and Type-C) in its interferometry measurement system which are designed based on the required sensitivity for each location of the mirror. Type-A isolation system is considered the main isolator system of the KAGRA which contains one IPP, five cascaded pendulum mechanical filters based Geometric-Anti Spring (GAS), and four cascaded pendulum masses for the cryogenic payload (platform mass, intermediate-mass, recoil mass, and mirror) [17].

Unlike LIGO (passive-active) approach, the Superattenuator or KAGRA (passive approach with IPP) isolator yielded a very low horizontal resonance frequency due to the IPP (about 70 mHz in KAGRA [17] and 40 mHz in Virgo [15]). In addition, the IPP provides means for positioning the entire isolation system and thus reducing the swinging angle of the optical payload. Beside, the IPP provides a point positioning system to compensate for the tidal drift [11, 4]. The experimental result of the Superattenuator for example shows about 10 orders of magnitude of isolation at 10 Hz [12]. Nevertheless, the isolation system of this approach is very long (10.5 m for Virgo [13], 13.5 m for KAGRA [17] and 17.5 m for ET [14]). This increases the complexity of compensating for any drift of the optical mirror or the entire isolation system. Also, such a large height increases the complexity of the infrastructure and adds extra cost to the system particularly if the system is to be mounted underground like ET [16, 18]. In addition, the passive isolation is achieved above the structure's resonances, which is not the case when applying active inertial control.

This study presents a compact isolation system that combines the features of having an active inertial platform, an IPP, and cascaded pendulum masses in one system. Adding the IPP to the isolation system yields a very low resonance frequency, provides means for the positioning of the entire isolation system and compensates for the tidal drift. On another side, the active inertial platform adds extra isolation in the low-frequency band (below 10 Hz), and yields more compact isolation system than a fully passive one. The cascaded pendulum masses are further used to suppress seismic noise at high frequency. By doing so, the model of the isolator should be able to provide an essential prediction performance, and also it should be valid for the control activities [2]. This new isolation system is carried out in the framework of the E-TEST project to investigate a new concept of design for the ET. This is because there is a high interest among the community of the ET to reduce the overall height of the proposed ET isolation system while maintaining the aforementioned performance requirements [19, 20, 14].

The design of this new isolation system and its output performance is demonstrated in this article as follows: section 2 presents the concept of the isolation system, section 3 demonstrates the applied control strategy, section 4 presents the result and the discussion of the closed-loop performance and lastly, the conclusion is presented in section 5.

## 2 Isolation system design

The schematic diagram of the compact isolation system is shown in Figure 1 (left). The isolation system consists of an Active inertail Platform (AP) that moves freely in 6 DOFs. The AP contains three springs aligned horizontally (x-axis or y-axis) and three springs aligned vertically (z-axis). This active inertail platform is designed on the success of the HAM-ISI active inertial platform [10]. The three legs of the Inverted Pendulum (IPL) are mounted on the AP and support the top stage (IPP). The interconnection of the IPLs with the AP and with the IPP is achieved by flexures. The horizontal resonance of the IPP is set to 0.07 Hz since such value can be experimentally obtained as demonstrated by KAGRA [17]. The Counter Weight (CW) is attached to each top-end of the IPL to improve the performance of the IPP by overcoming the physical phenomenon that is called the center of percussion where the isolation starts to saturate at a certain level of attenuation [11]. The GAS filter after that is housed in the IPP for vertical isolation. From the GAS filter, a Marionette (Mar) is suspended which is mainly used to position the payload. The payload contains the Cold Platform (CP) and the Mirror (Mir) in which the Mir is hanging from CP via 4 wires. The overall suspension system is about 4.5 m in height. This compact isolation system is a full scale with a 100 kg silicon mirror.

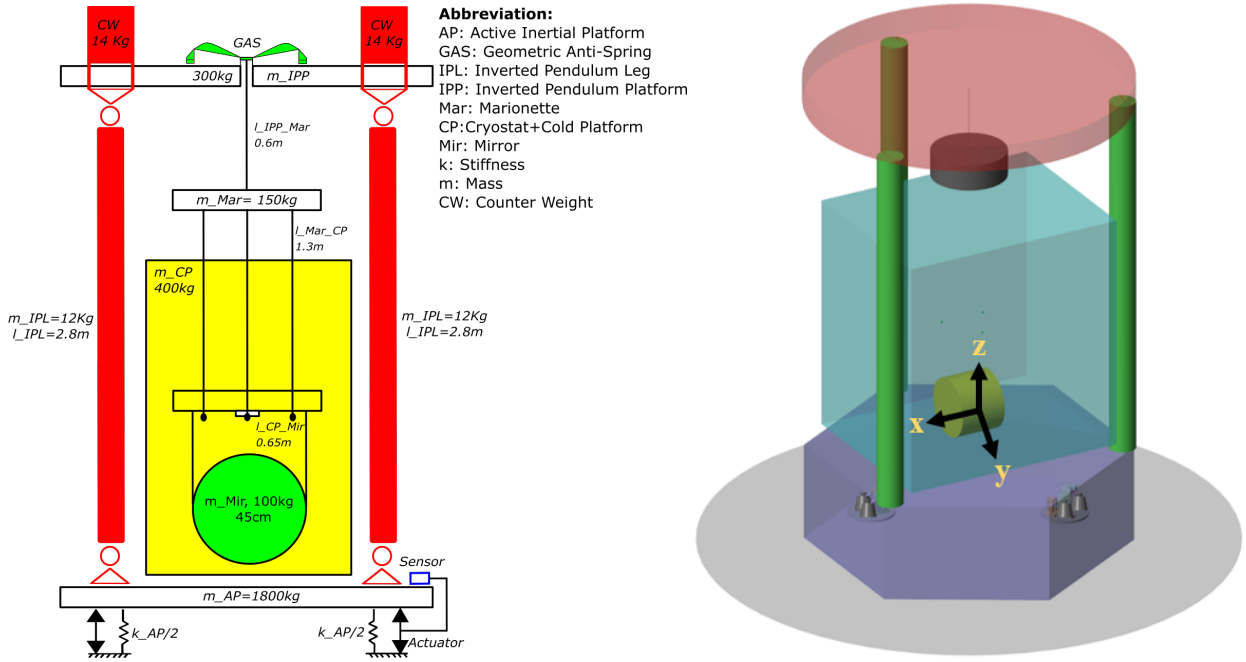


Figure 1: Isolation System: Schematic Model (Left) and 3D View Simscape Model (Right).

To study the dynamics of the prototype in 3D, a multi-body model has been developed using Simscape. It is a Matlab toolbox allowing to study of lumped mass systems under gravity. Since it works under the Simulink environment, it is also a convenient tool for extracting the state space of the model and implementing feedback control strategies. A 3D view of the Simscape model is further shown in Figure 1 (right).

## 3 Applied control strategy

A schematic diagram for the AP of the isolation system is shown in Figure 2. It contains six actuators (3 for horizontal directions and 3 for vertical directions) and six inertial sensors (3 for horizontal directions (Horizontal Interferometric Inertial Sensor (HINS)) and 3 for vertical directions (Vertical Interferometric Inertial Sensor (VINS)). These inertial sensors, demonstrated in [21], are based on an interferometric readout.

The transfer function of each pair of the sensor/actuator are shown in Figure 3. These curves have been extracted from the full model. Due to the symmetry, the three vertical ones are identical and the three

horizontal ones are identical as well. For the horizontal direction, the first resonance and anti-resonance appear at 0.07 Hz and 0.13 Hz, respectively. These represent the resonance of the IPP and its coupling due to the differences in the position of the Center of Mass (COM) of the IPP and the COM of the AP. Then the resonance of the inertial sensor is at 0.2 Hz. Followed by that, two resonances and one anti-resonance are around 1 Hz. These represent the resonance of the AP and its associated couplings that results from the sensors and actuators being not located at the COM of the AP. The order of the resonances in the vertical direction is similar to the horizontal directions.

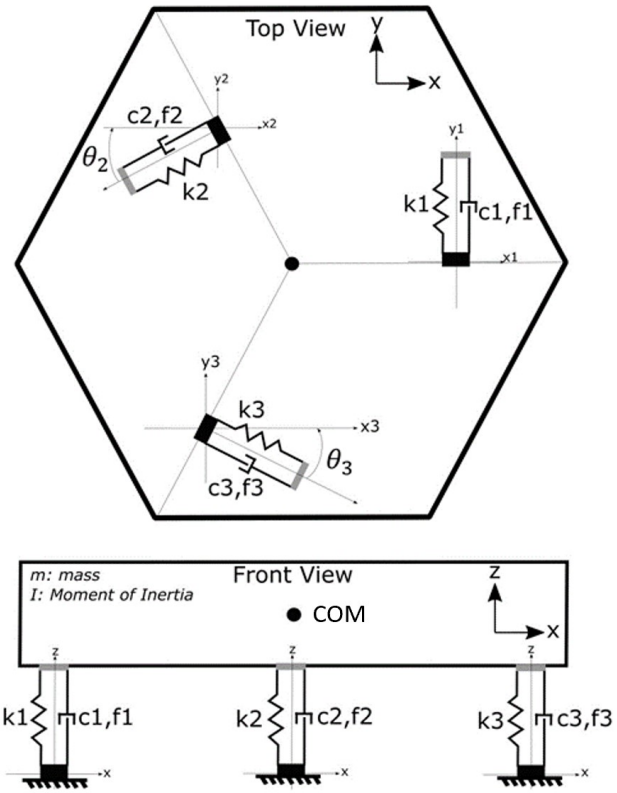


Figure 2: Active Inertial Platform.

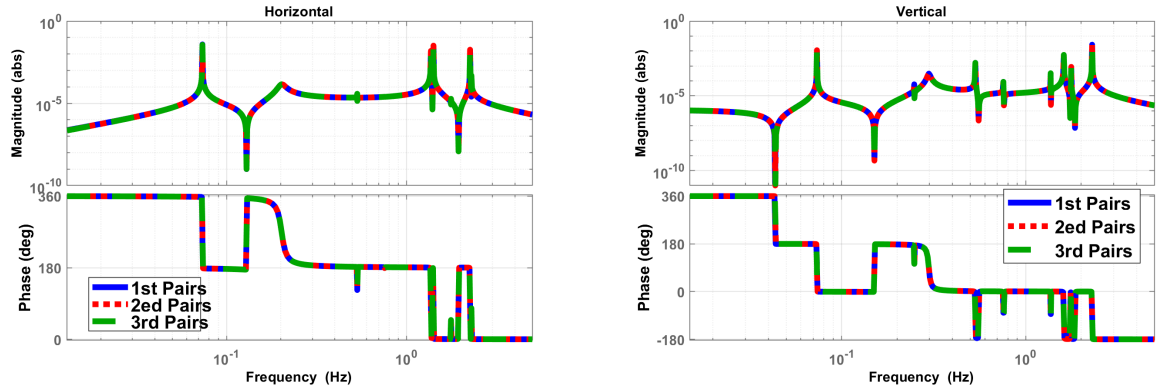


Figure 3: Transfer Function of Each Sensor/Actuator Pair of the Active Inertial Platform.

The off-diagonal elements of the transfer matrix, shown in Figure 4, are of the same order of magnitude as the diagonal ones. To control the platform, a decoupling strategy has to be applied.

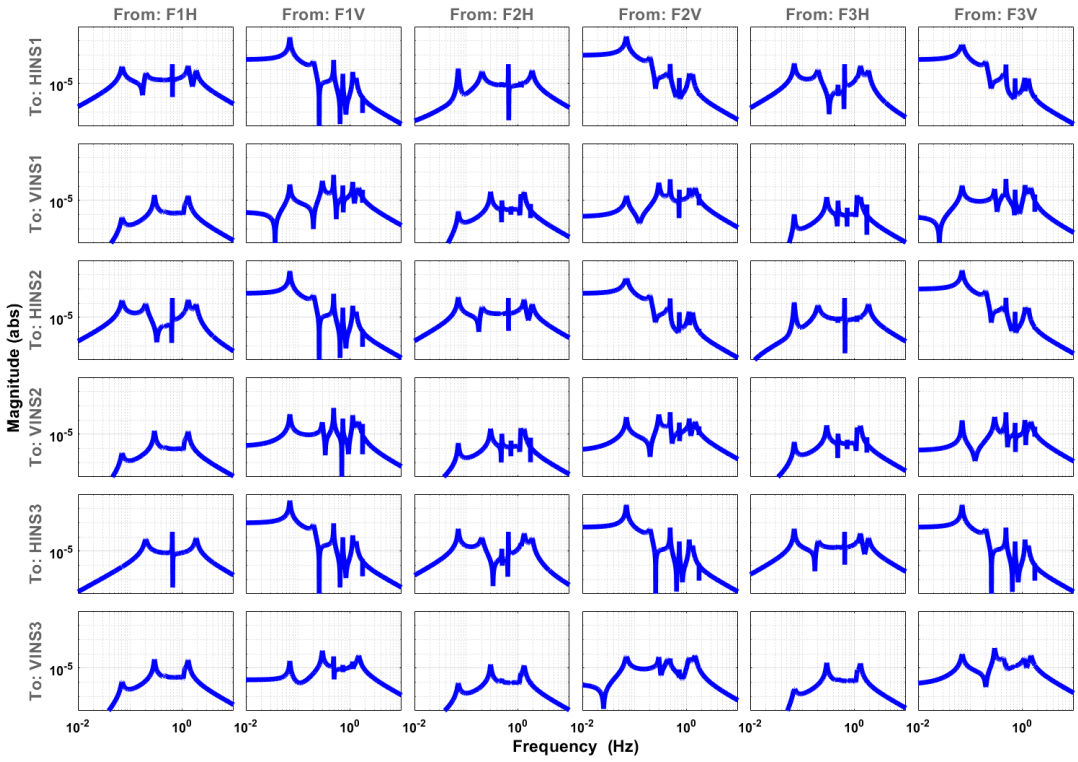


Figure 4: Transfer Matrix of Coupled System.

This study applies a decoupling strategy based on a Jacobian approach to minimize the coupling and move from the local frame to the Cartesian frame of the AP. This is schematically represented in Figure 5, where $J_a$ is the actuator Jacobian and $J_s$ is the sensor Jacobian. These Jacobian matrices depend on the geometry of the AP and the position of the sensors and actuators on it. The decoupling frame can either be at the COM of AP which yields a diagonal mass matrix (good decoupling at high frequency) or at the Center of Stiffness (COK) which yields a diagonal stiffness matrix (good decoupling at low frequency). The ideal condition for the decoupling is where we obtain both at the same time: diagonal mass matrix and diagonal stiffness matrix. This occurs when the COM and COK are geometrically designed to be at the same location. However, this is not the case for the current isolation system. This is because the safety tubes (surrounding IPLs and mounted on the AP) add extra inertia to the AP hence shifting the COM of AP outside its geometry. On the other side, the COK can not be designed outside the geometry of AP. Therefore, the COK is selected as a decoupling frame since the bandwidth of interest is at a low frequency.

Once the plant is decoupled, each degree of freedom can be controlled individually as shown in the same figure. The poles and zeros of the controllers are designed based on a manual tuning (loop shaping) in the SISO tool - Matlab. This method is efficient in terms of understanding the behavior of the system and also the positions of the poles/zeros of the controller. The designed controllers are further demonstrated in Figure 6. In the plot, x and y represent the translation horizontal direction whereas z represents the translation vertical direction. The xr and yr represent the rotational horizontal direction and zr represents the rotational vertical direction. The magnitudes of the designed controllers are considered realistic where such magnitude is experimentally obtained in the PML (Precision Mechatronics Laboratory) as shown in the article [22].

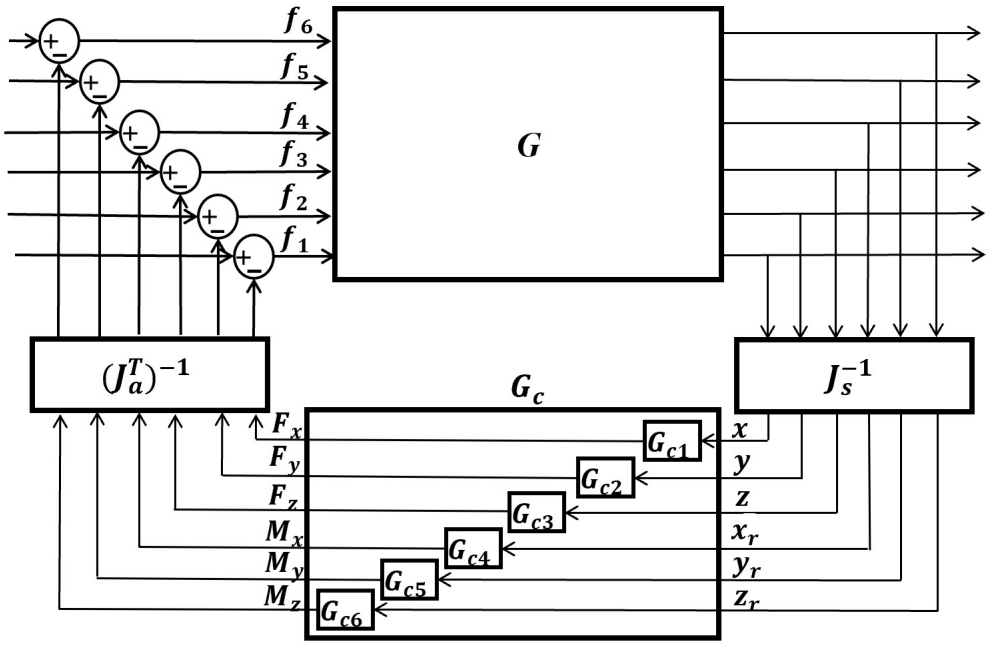


Figure 5: Schematic Representation of the Centralized Control of the AP.

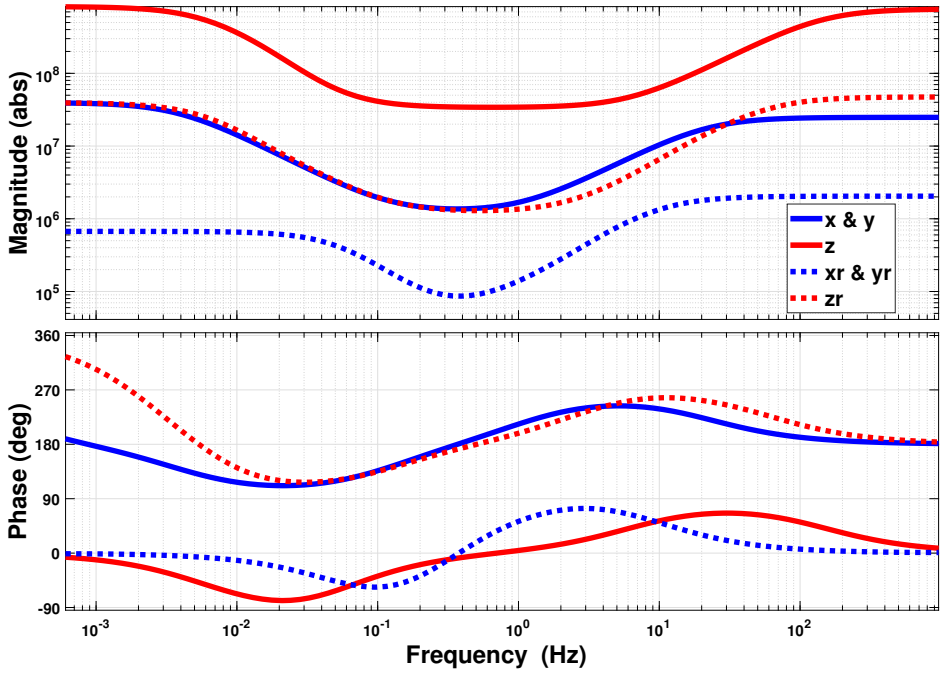


Figure 6: Controller Design for the Closed Loop System of the E-TEST.

## 4 Results and discussion

The magnitude of the off-diagonal elements of the transfer matrix, shown in Figure 7, are now reduced after applying the decoupling strategy. However, there is still a residual coupling for the horizontal rotational

directions (xr-axis and yr-axis) when applying a horizontal force. This is a result of not having the COM and the COK in the same frame. The magnitude of these couplings will be smaller if the COM and the COK are designed within the same frame. In addition, there is also a residual coupling for the horizontal directions (x-axis and y-axis) when applying a torsion in the same directions. This is due to the residual coupling of the inertial sensor as they do not distinguish between rotational motion and translational motion. This is caused by the coupling between the mechanics of the sensor (spring-mass) and the gravity force [23]. Overall, the control of the platform can now be applied with this low magnitude of the off-diagonal elements in comparison with the diagonal elements.

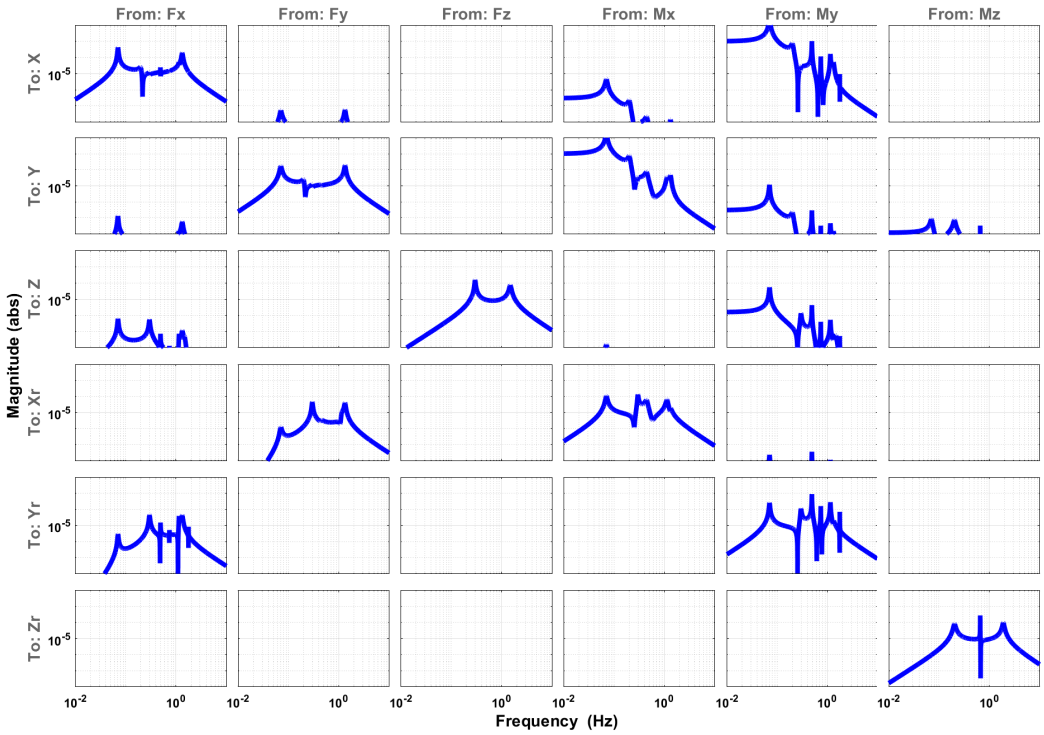


Figure 7: Transfer Matrix of the Decoupled Systems (AP alone and Entire E-TEST) with Implementing Sensor Dynamics (Inertial Sensor).

Figure 8 compares the open-loop and the closed-loop transmissibilities from the ground to the AP in vertical (z-axis) and horizontal (x-axis) directions. The figure shows that the transmitted motion is reduced by about two orders of magnitude when the inertial control is switched on. Not surprisingly, the same reduction is also visible in the transmissibilities from the ground to the mirror as shown in Figure 9. In total, this new passive-active isolator yields about three orders of magnitude of the seismic noise reduction at 1 Hz in the vertical and horizontal directions.

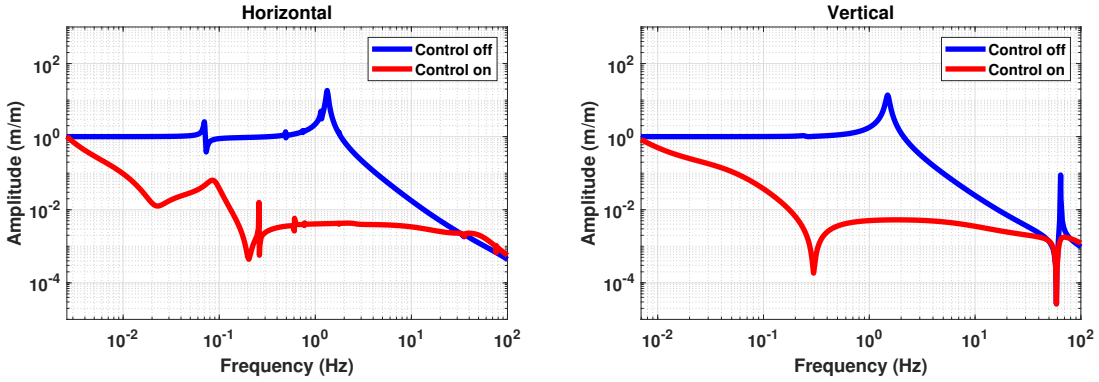


Figure 8: Transmissibilities from Ground to AP.

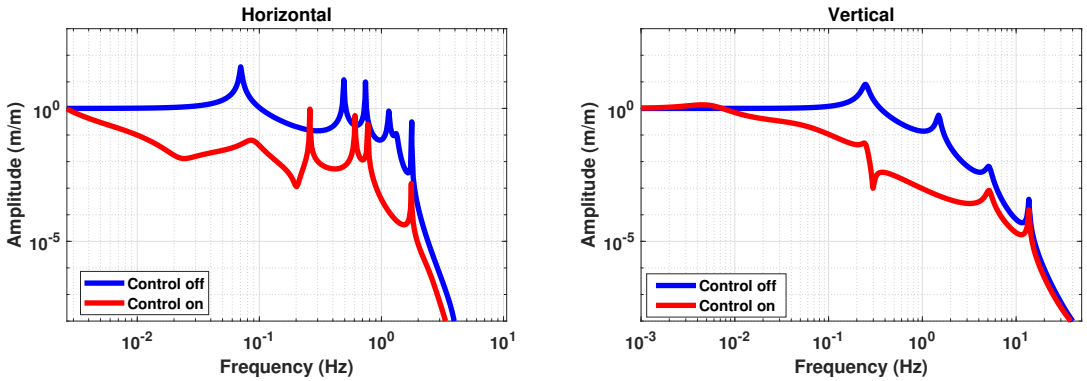


Figure 9: Transmissibilities from Ground to Mirror.

Despite of the residual inertail sensor coupling, the control is still performing well. This is further depicted in Figure 10 which shows the transfer matrix for the open and closed loop systems.

Moreover, the ASD (Amplitude Spectral Density) of the AP as well as of the mirror are illustrated respectively in Figures 11 and 12. For reference, the noise floor of the in-loop sensors is also shown in the same figure. It is seen that the closed-loop performance of the system is not limited by the sensor resolution. Instead, there is extra room for better performance if a more aggressive controller is applied. The limitation of the tilt ground coupling is not discussed in this article.

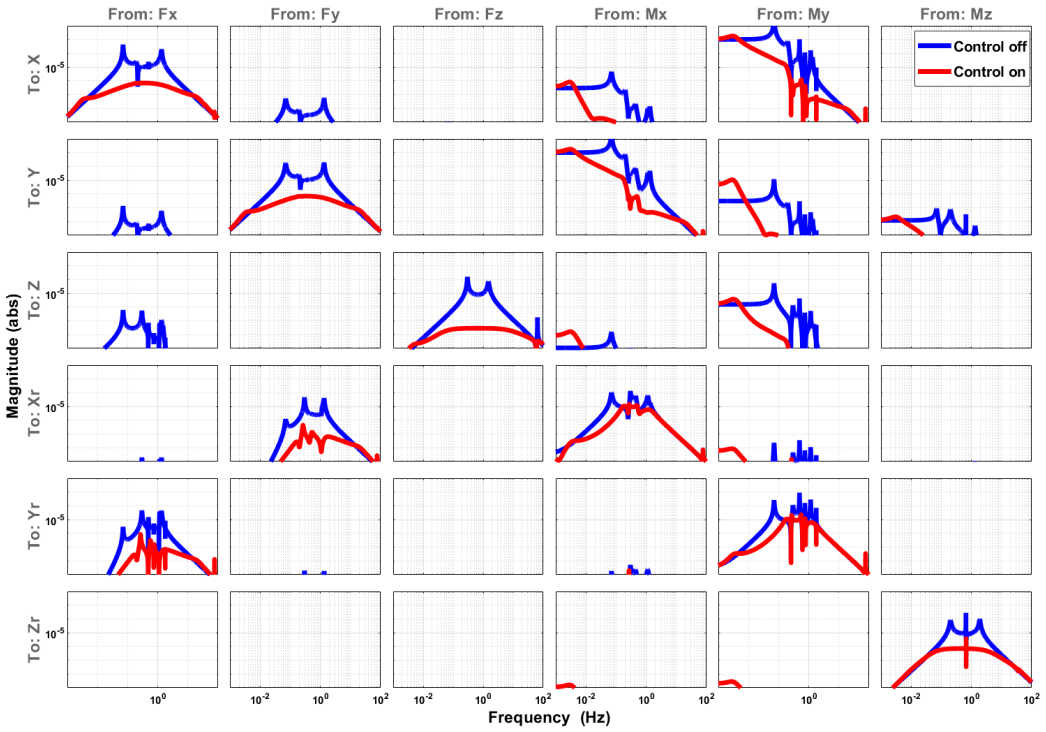


Figure 10: Transfer Matrix Of the Open Loop and Closed Loop of the E-TEST.

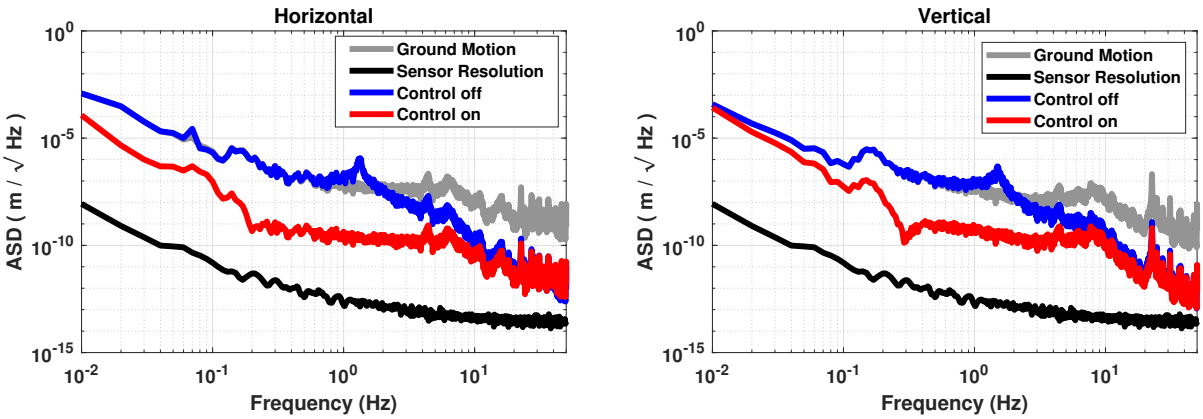


Figure 11: ASD of the Active Platform Motion, the Sensor Noise and the Ground Motion at CSL.

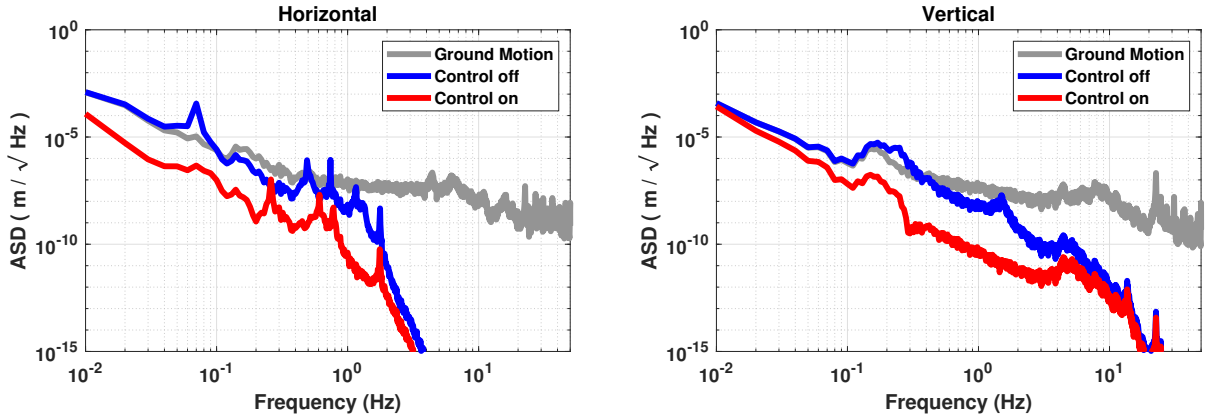


Figure 12: ASD of the Mirror and the Ground Motions at CSL.

## 5 Conclusion

This study presented a new approach for the isolation of a large mirror at low frequency. It showed the potential advantages of having such an approach by combining an active inertial platform with a passive IPP and multi-cascaded pendulums. This yielded a compact isolator system with seismic noise suppression at low frequency (below the structure's resonances) which is not the case if only a passive isolator is used. Also, the study showed the efficient of the applied control strategy to firstly reduce the magnitude of the off-diagonal elements of the transfer matrix and then apply a controller in the Cartesian frame based on the loop shaping method. Though the residual coupling of the inertial sensor, the control strategy is still operating. In addition, the closed-loop performance of the system was not limited by the sensor noise, instead, there is room for improving closed-loop performance. The simulation result showed a seismic noise reduction by about 3 orders of magnitude at 1 Hz for horizontal and vertical directions. The applied controller was based on a manual tuning (loop shaping) which is considered time-consuming and the controller sometimes needs to be re-designed for any parameter changes. Therefore, a more advanced control strategy, for example, loop shaping based on H-infinity, can be further applied which can define the optimal controller parameters automatically based on the given specifications and restrictions. In addition, the inertial platform should be designed in such a way that the first flexible internal mode appears above 300 Hz to avoid spoiling the control performance at high frequency,

## Acknowledgements

This work comes within the scope of the E-TEST project which is carried out within the framework of the Interreg V-A Euregio Meuse-Rhine Programme, with € 7,5 million from the European Regional Development Fund (ERDF). By investing EU funds in Interreg projects, the European Union is investing directly in economic development, innovation, territorial development, social inclusion, and education in the Euregio Meuse-Rhine. For a thorough review, the authors would like to thank European Union for this support and investment.

## References

[1] M. Granata, M. Barsuglia, R. Flaminio, A. Freise, S. Hild, and J. Marque, "Design of the advanced virgo non-degenerate recycling cavities," *Journal of Physics: Conference Series*, vol. 228, no. 1, p. 012016, 2010.

[2] F. Matichard, B. Lantz, K. Mason, R. Mittleman, B. Abbott, S. Abbott, E. Allwine, S. Barnum, J. Birch, S. Biscans *et al.*, "Advanced ligo two-stage twelve-axis vibration isolation and positioning platform. part 1: Design and production overview," *Precision Engineering*, vol. 40, pp. 273–286, 2015.

[3] T. Ushiba, T. Akutsu, S. Araki, R. Bajpai, D. Chen, K. Craig, Y. Enomoto, A. Hagiwara, S. Haino, Y. Inoue *et al.*, "Cryogenic suspension design for a kilometer-scale gravitational-wave detector," *Classical and Quantum Gravity*, vol. 38, no. 8, p. 085013, 2021.

[4] M. Abernathy *et al.*, "in preparation."

[5] G. M. Harry, L. S. Collaboration *et al.*, "Advanced ligo: the next generation of gravitational wave detectors," *Classical and Quantum Gravity*, vol. 27, no. 8, p. 084006, 2010.

[6] M. Granata, M. Barsuglia, R. Flaminio, A. Freise, S. Hild, and J. Marque, "Design of the advanced virgo non-degenerate recycling cavities," in *Journal of Physics: Conference Series*, vol. 228, no. 1. IOP Publishing, 2010, p. 012016.

[7] B. P. Abbott, R. Abbott, T. Abbott, S. Abraham, F. Acernese, K. Ackley, C. Adams, V. Adya, C. Affeldt, M. Agathos *et al.*, "Prospects for observing and localizing gravitational-wave transients with advanced ligo, advanced virgo and kagra," *Living reviews in relativity*, vol. 23, no. 1, pp. 1–69, 2020.

[8] F. Matichard, B. Lantz, R. Mittleman, K. Mason, J. Kissel, B. Abbott, S. Biscans, J. McIver, R. Abbott, S. Abbott *et al.*, "Seismic isolation of advanced ligo: Review of strategy, instrumentation and performance," *Classical and Quantum Gravity*, vol. 32, no. 18, p. 185003, 2015.

[9] S. Aston, M. Barton, A. Bell, N. Beveridge, B. Bland, A. Brummitt, G. Cagnoli, C. Cantley, L. Carbone, A. Cumming *et al.*, "Update on quadruple suspension design for advanced ligo," *Classical and Quantum Gravity*, vol. 29, no. 23, p. 235004, 2012.

[10] J. S. Kissel, "Calibrating and improving the sensitivity of the ligo detectors," 2010.

[11] A. Takamori, "Low frequency seismic isolation for gravitational wave detectors," *University of Tokyo*, 2002.

[12] T. Accadia, F. Acernese, F. Antonucci, P. Astone, G. Ballardin, F. Barone, M. Barsuglia, T. S. Bauer, M. Beker, A. Belletoile *et al.*, "The seismic superattenuators of the virgo gravitational waves interferometer," *Journal of low frequency noise, vibration and active control*, vol. 30, no. 1, pp. 63–79, 2011.

[13] F. a. Acernese, M. Agathos, K. Agatsuma, D. Aisa, N. Allemandou, A. Allocca, J. Amarni, P. Astone, G. Balestri, G. Ballardin *et al.*, "Advanced virgo: a second-generation interferometric gravitational wave detector," *Classical and Quantum Gravity*, vol. 32, no. 2, p. 024001, 2014.

[14] F. Acernese, *et al.*, and "Einstein Telescope Science Team", "Einstein gravitational wave telescope conceptual design study," "https://tds.virgo-gw.eu/?call_file=ET-0106C-10.pdf", 2011.

[15] T. Accadia, F. Acernese, F. Antonucci, P. Astone, G. Ballardin, F. Barone, M. Barsuglia, T. S. Bauer, M. G. Beker, A. Belletoile, S. Birindelli, M. Bitossi, M. A. Bizouard, M. Blom, C. Boccara, F. Bondu, L. Bonelli, R. Bonnand, V. Boschi, L. Bosi, B. Bouhou, S. Braccini, C. Bradaschia, A. Brillet, V. Brisson, R. Budzynski, T. Bulik, H. J. Bulten, D. Buskulic, C. Buy, G. Cagnoli, E. Calloni, E. Campagna, B. Canuel, F. Carbognani, F. Cavalier, R. Cavalieri, G. Cella, E. Cesarini, E. Chassande-Mottin, A. Chincarini, F. Cleva, E. Coccia, C. N. Colacino, J. Colas, A. Colla, M. Colombini, A. Corsi, J. P. Coulon, E. Cuoco, S. D'Antonio, V. Dattilo, M. Davier, R. Day, R. De Rosa, G. Debreczeni, M. del Prete, L. Di Fiore, A. Di Lieto, M. Di Paolo Emilio, A. Di Virgilio, A. Dietz, M. Drago, V. Fafone, I. Ferrante, F. Fidecaro, I. Fiori, R. Flaminio, J. D. Fournier, J. Franc, S. Frasca, F. Frasconi, A. Freise, M. Galimberti, L. Gammaitoni, F. Garufi, M. E. Gáspár, G. Gemme, E. Genin, A. Gennai, A. Giazotto, R. Gouaty, M. Granata, C. Greverie, G. M. Guidi, J. F. Hayau, H. Heitmann, P. Hello, S. Hild, D. Huet, P. Jaranowski, I. Kowalska, A. Krolak, N. Leroy, N. Letendre, T. G. F. Li, M. Lorenzini, V. Loriette,

G. Losurdo, E. Majorana, I. Maksimovic, N. Man, M. Mantovani, F. Marchesoni, F. Marion, J. Marque, F. Martelli, A. Masserot, C. Michel, L. Milano, Y. Minenkov, M. Mohan, J. Moreau, N. Morgado, A. Morgia, S. Mosca, V. Moscatelli, B. Mours, I. Neri, F. Nocera, G. Pagliaroli, L. Palladino, C. Palomba, F. Paoletti, S. Pardi, M. Parisi, A. Pasqualetti, R. Passaquieti, D. Passuello, G. Persichetti, M. Pichot, F. Piergiovanni, M. Pietka, L. Pinard, R. Poggiani, M. Prato, G. A. Prodi, M. Punturo, P. Puppo, D. S. Rabeling, I. Rácz, P. Rapagnani, V. Re, T. Regimbau, F. Ricci, F. Robinet, A. Rocchi, L. Rolland, R. Romano, D. Rosinska, P. Ruggi, B. Sassolas, D. Sentenac, L. Sperandio, R. Sturani, B. Swinkels, A. Toncelli, M. Tonelli, O. Torre, E. Tournefier, F. Travasso, G. Vajente, J. F. J van den Brand, S. van der Putten, M. Vasuth, M. Vavoulidis, G. Vedovato, D. Verkindt, F. Vetrano, A. Viceré, J. Y. Vinet, H. Vocca, M. Was, and M. Yvert, "The seismic Superattenuators of the Virgo gravitational waves interferometer," *Low Frequency Noise, Vibration and Active Control*, vol. 30, no. 1, pp. 63–79, Jun. 2011.

[16] T. Akutsu, M. Ando, K. Arai, Y. Arai, S. Araki, A. Araya, N. Aritomi, H. Asada, Y. Aso, S. Bae *et al.*, "Vibration isolation systems for the beam splitter and signal recycling mirrors of the kagra gravitational wave detector," *Classical and Quantum Gravity*, vol. 38, no. 6, p. 065011, 2021.

[17] K. OKUTOMI *et al.*, "Development of 13.5-meter-tall vibration isolation system for the main mirrors in kagra," 2019.

[18] S. Di Pace, V. Mangano, L. Pierini, A. Rezaei, J.-S. Hennig, M. Hennig, D. Pascucci, A. Allocca, I. Tosta e Melo, V. G. Nair *et al.*, "Research facilities for europe's next generation gravitational-wave detector einstein telescope," *Galaxies*, vol. 10, no. 3, p. 65, 2022.

[19] E. steering committee, "Et design report update 2020," 2020.

[20] G. P Ruggi, "Thoughts on the seismic isolation for et," 2019.

[21] B. Ding, G. Zhao, J. Watchi, A. Sider, and C. Collette, "An interferometric inertial sensor for low-frequency seismic isolation," *Sensors and Actuators A: Physical*, vol. 335, p. 113398, 2022.

[22] G. Zhao, B. Ding, J. Watchi, A. Deraemaeker, and C. Collette, "Experimental study on active seismic isolation using interferometric inertial sensors," *Mechanical Systems and Signal Processing*, vol. 145, p. 106959, 2020.

[23] C. Collette, S. Janssens, P. Fernandez-Carmona, K. Artoos, M. Guinchard, C. Hauviller, and A. Preumont, "Inertial sensors for low-frequency seismic vibration measurement," *Bulletin of the seismological society of America*, vol. 102, no. 4, pp. 1289–1300, 2012.

# Appendix

## A Nomenclature

| | |
|---|---|
| $IPP$ | Inverted Pendulum Platform |
| $GW$ | Gravitational Wave |
| $IP$ | Inverted Pendulum |
| $IPL$ | Inverted Pendulum Leg |
| $GW$ | Gravitational Wave |
| $AP$ | Active inertail Platform |
| $GAS$ | Geometric-Anti Spring |
| $Mar$ | Marionette |
| $CP$ | Cold Platform |
| $Mir$ | Mirror |
| $K$ | Stiffness |
| $m$ | mass |
| $CW$ | Counter Weight |
| $D$ | Dimension |
| $HINS$ | Horizontal Interferometric Inertial Sensor |
| $VINS$ | Vertical Interferometric Inertial Sensor |
| $I$ | Moment of Inertia |
| $c$ | Damping Coefficient |
| $COM$ | Center of Mass |
| $f$ | Applied Force |
| $G$ | Plant |
| ${J_a}^{-1}$ | Actuator Jacobian |
| ${J_s}^{-1}$ | Sensor Jacobian |
| $ASD$ | Amplitude Spectral Densities |